ACS Catalysis

Letter

pubs.acs.org/acscatalysis

Noble-Metal-Free NO_x Storage over Ba-Modified TiO_2 Photocatalysts under UV-Light Irradiation at Low Temperatures

Akira Yamamoto,[†] Yuto Mizuno,[†] Kentaro Teramura,*[,†,‡,§] Saburo Hosokawa,[†,‡] and Tsunehiro Tanaka*[,†,‡,§]

[†]Department of Molecular Engineering, Graduate School of Engineering, Kyoto University, Kyotodaigaku Katsura, Nishikyo-ku, Kyoto 615-8510, Japan

[‡]Elements Strategy Initiative for Catalysts & Batteries (ESICB), Kyoto University, Kyotodaigaku Katsura, Nishikyo-ku, Kyoto 615-8520, Japan

[§]Precursory Research for Embryonic Science and Technology (PRESTO), Japan Science and Technology Agency (JST), 4-1-8 Honcho, Kawaguchi, Saitama 332-0012, Japan

Supporting Information

ABSTRACT: Photoassisted nitrogen oxide (NO_x) storage was investigated over the barium-modified titanium dioxide (Ba/TiO_2) photocatalysts under UV-light irradiation at a high concentration of nitrogen monoxide (NO) of 200 ppm and a high gas hourly space velocity (GHSV) of 50 000 h^{-1}. The NO removal efficiency was kept >99% during the 1020 s interval from the start of the reaction over the Ba/TiO_2 photocatalyst. The temperature-programed desorption (TPD) measurement and X-ray diffraction (XRD) technique revealed that barium oxide (BaO) species functioned as a NO_x storage material even at low temperatures, which result in improvement of the performance of the photoassisted NO_x storage.

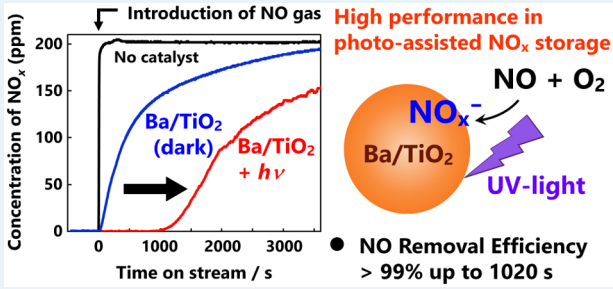

KEYWORDS: *photocatalyst, nitrogen oxides, NO_x, titanium dioxide, barium, NO_x storage, lean NO_x trap*

Lean-burn and diesel engines are one of the most important technologies to improve the fuel efficiency of internal combustion engines and reduce carbon dioxide (CO_2) emissions. Significant fuel economy can be achieved when the engines operate under lean conditions of an air-to-fuel (A/F) ratio of approximately 20−65.[1] The conventional three-way catalyst is not capable of efficiently decomposing NO_x in the exhaust gas from the engines, although it can reduce NO_x in the stoichiometric condition at an A/F ratio of 14.7.[2,3] The NO_x removal at high A/F ratios was performed using catalytic processes such as selective catalytic reduction (SCR)[4,5] and NO_x storage and reduction (NSR).[6−8]

In the SCR system, urea is injected into the exhaust gas and decomposes into ammonia (NH_3) and CO_2. The NH_3 reacts with NO_x in the exhaust gas to form harmless nitrogen (N_2) under the lean condition. This technology is widely used in diesel engines and motor vehicles using Fe- or Cu-zeolite catalysts.[9−13] Alternatively, the NSR catalyst (typically, Pt/BaO/Al_2O_3) operates under lean and rich conditions. NO_x was oxidized over Pt and stored as nitrite (NO_2^-) or nitrate (NO_3^-) species under the lean condition, where barium oxide (BaO) functions as a NO_x storage material.[14] After the NO_x storage period under the lean condition (approximately 60−90 s), the engines are switched to the fuel-rich condition for a short period (approximately 3−5 s) by injecting fuels, where the stored NO_x is released and reduced into harmless N_2 over Pt.[14] The cycling operation of the lean and rich conditions provides high NO_x removal efficiency.[15] However, these SCR and NSR catalysts cannot reduce NO_x efficiently below 423 K.[16−18] In the urea-SCR system, according to the reports of the International Council for Clean Transportation (ICCT), urea injection could not start for approximately 800 s during the cold start test in the world harmonized transient cycle (WHTC) because the temperature of the exhaust gas was too low.[16] Controlling the NO_x emission under the cold start condition is a key and urgent task to lower the total emission of NO_x.

We have focused on TiO_2 photocatalysts as NO_x storage materials to reduce NO_x emissions in the cold start condition from the viewpoint of nontoxicity, low operating temperature, and rapid response to light. Under the cold start condition, utilizing the photocatalysts enable the de-NO_x system to work at the same time that the engine starts. There are many reports concerning the oxidation of NO over TiO_2-based photocatalysts under light irradiation.[19−28] In these reports, NO in the gas phase was oxidized to NO_2 and surface NO_x^- species

Received: January 24, 2015
Revised: April 7, 2015
Published: April 9, 2015

DOI: 10.1021/acscatal.5b00151
ACS Catal. 2015, 5, 2939−2943

and stored on the TiO_2 surface. Most of the researchers investigated the oxidation of NO over TiO_2 photocatalysts at very low concentrations of NO (less than 10 ppm) and/or at low gas hourly space velocity (GHSV) of 10−1000 h^{-1} because their objective was the removal of NO_x in air[22,29] and elucidation of the reaction mechanism of NO oxidation.[24,25,30−32] These conditions were quite different from those of practical exhaust gas in lean-burn engines (typically, concentration of NO > 200 ppm and GHSV > 50 000 h^{-1}). Thus, the potential of the TiO_2 photocatalyst for NO_x storage materials in the cold start condition has not been investigated. In this research, we investigated photoassisted NO_x storage at a high concentration of NO and high GHSV to assess the potential of the TiO_2 photocatalyst. In addition, the role of Ba modification was examined in the performance of the photoassisted NO_x storage.

Anatase TiO_2 powder with a high surface area (ST-01, anatase, 292 m^2 g^{-1}) was used in this study. Ba-modified TiO_2 (Ba/TiO_2) was prepared using a simple impregnation method using $Ba(NO_3)_2$ as a precursor. Photoassisted NO_x storage was performed using a conventional fixed bed flow system under atmospheric pressure. A quartz reactor (H12 mm × W10 mm × D1.0 mm, the reactor volume: 0.12 mL) was used for the reaction, and 0.13 g of catalyst granules were introduced into the reactor and then pretreated at various temperatures (298−873 K) in a 10% O_2/He gas mixture at a flow rate of 50 mL min^{-1} for 1 h. The reaction gas composition was as follows: NO (200 ppm), O_2 (3%), and He (balance). A 300-W Xe lamp (PerkinElmer PE300BF) was used as the light source. The outlet concentration of NO_x ($NO + NO_2$) was measured using a portable gas analyzer (HORIBA PG-335). The reaction temperature was monitored by using a thermocouple.

Figure 1 shows the time course of the outlet concentrations of NO_x (= $NO + NO_2$) for NO_x storage under various reaction conditions after the pretreatment at 773 K in a 10% O_2/He gas mixture. The reaction temperature increased up to 373 K after the start of the light irradiation, and it was stable during the reaction. without a catalyst, the concentration of NO_x increased with the introduction of NO and immediately became 200 ppm. However, the concentration of NO was less than 2 ppm during the initial 530 s of the reaction (conversion of NO > 99%) over TiO_2. After the dead time for the breakthrough of NO_x, the concentration of NO gradually increased with the reaction time and became 175 ppm after 3 h (not saturated), where N_2 and N_2O products were not detected by the TCD-GCs. (In this research, the dead time for the breakthrough of NO_x was defined as the time at which the concentration of NO_x exceeded 2 ppm (99% of the conversion of NO) in the outlet gas.) The concentration of NO became 200 ppm after 20 h of the reaction (see Figure S1 in SI), where the inlet NO gas slipped through the catalyst possibly because of the saturation of the TiO_2 surface by the adsorbed NO_x species. The total amount of the stored NO_x species after 20 h was calculated to be 426 μmol g^{-1} from Figure S1. The surface density of NO_x species was calculated to be 1.4 nm^{-2}. When the TiO_2 (100) surface is considered, the density of the surface Ti atoms was 7.0 nm^{-2}, and 20% of the surface Ti sites are occupied by the adsorbed NO_x species assuming a one-to-one relationship between the stored NO_x species and surface Ti sites.

The addition of Ba drastically enhanced the dead time of the NO_x slip to 1020 s, which was almost twice as long as that of the TiO_2 photocatalyst. The dead time value meets the demand (800 s) for the cold start condition reported by the ICCT.[16]

The NO_x storage capability (NSC) is defined as the amount of stored NO_x after 1 h from the start of the reaction and was calculated to be 252 μmol g^{-1}. For the typical NSR catalyst, $Pt/Ba/Al_2O_3$, the NSC at 473 and 573 K was reported to be 177 and 581 μmol g^{-1}, respectively.[7] The NSC of the Ba/TiO_2 photocatalyst was comparable to that of the typical NSR catalyst containing precious noble metals (Pt). Thus, the utilization of photocatalysts enables us to eliminate the use of expensive and rare precious metals from the de-NO_x catalyst.

The NO_x storage under light irradiation proceeds via the following equations according to the previous reports.[25,33]

$$NO \xrightarrow{O_2,h\nu} NO_2 \quad (1)$$

$$NO_2 \xrightarrow{O_2,dark} NO_2^-, NO_3^- \quad (2)$$

$$NO \xrightarrow{O_2,dark} NO_2^-, NO_3^- \quad (3)$$

$$NO_2^- \xrightarrow{O_2,h\nu} NO_3^- \quad (4)$$

In the dark, the activity of the NO_x storage was low (no dead time), as shown in Figure 1c, although the NO_x storage

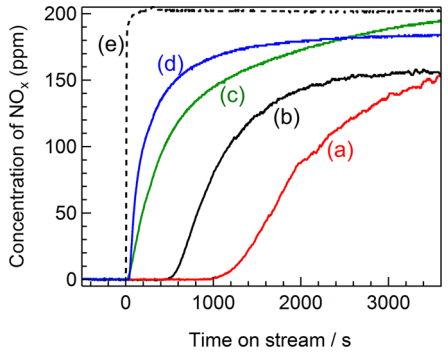

Figure 1. Time course of the NO_x storage under various reaction conditions after the pretreatment at 773 K. (a): over 500 μmol g^{-1} Ba/TiO_2 catalyst under UV-light irradiation, (b): over TiO_2 catalyst under UV-light irradiation, (c): over 500 μmol g^{-1} Ba/TiO_2 catalyst in the dark, (d): over 500 μmol g^{-1} Ba/TiO_2 catalyst under UV-light irradiation without O_2 gas, and (e): without catalyst.

proceeded to some extent, and the NSC was calculated to be 88.4 μmol g^{-1}. Previous IR investigations revealed that NO_2^- and NO_3^- species were generated on a TiO_2 surface after NO + O_2 coadsorption in the dark (eq 3).[33,34] The NO_x storage in the dark was possibly due to the oxidation and adsorption of NO represented in eq 3. The reaction hardly proceeded in the absence of O_2 (Figure 1d), which means O_2 molecules involve in the NO_x storage. Active oxygen radicals such as O_2^-, O_3^-, and O^-, which are generated on TiO_2 under UV-light irradiation, oxidize NO and NO_2^- into NO_3^- species according to eqs 1 and 4.[24,25,29] Thus, the oxidation of NO and/or NO_2^- species is accelerated by UV-light irradiation, which is likely to result in the high activity under UV-light irradiation. In addition, the reusability of Ba/TiO_2 was investigated after the pretreatment at 773 K (the experimental detail and the result are shown in SI). Marked deactivation was not observed, which suggests that the stored NO_x species decompose after the pretreatment at 773 K. We concluded that the catalyst is regenerable and reusable by the pretreatment.

Figure 2 shows the time course of the NO_x storage at various pretreatment temperatures over the TiO_2 and Ba/TiO_2

DOI: 10.1021/acscatal.5b00151
ACS Catal. 2015, 5, 2939−2943

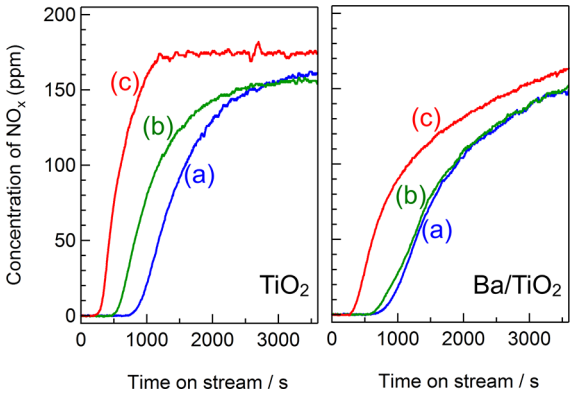

Figure 2. Time course of the NO_x storage at the pretreatment temperatures of 673 K (a), 773 K (b), and 873 K (c). NO: 200 ppm, O_2: 3%, He balance.

catalysts. The NSC and dead time drastically decreased with the pretreatment temperature using the TiO_2 photocatalyst. Only the diffraction pattern of anatase TiO_2 was observed in the XRD patterns of all the TiO_2 samples before and after the reaction (Figure S3). As observed in Table 1 (entries 1−3), the crystalline size of TiO_2 increased from 8.9 to 28 nm, and the specific surface area (SSA) of the catalysts decreased from 292 to 50.7 $m^2\ g^{-1}$ after the pretreatment at 873 K. The positive correlation of the NSC and SSA strongly indicates that the SSA has a significant effect on the NSC for the TiO_2 photocatalyst.

Ba/TiO_2 exhibits high resistance to the high-temperature pretreatment; the decrease in the activity of the Ba/TiO_2 catalysts by elevating the pretreatment temperature was smaller than that observed for the TiO_2 catalyst (Figure 2 and entries 8, 10, and 11 in Table 1). The SSA of the Ba/TiO_2 catalyst was almost stable up to 773 K and then decreased at 873 K. The pretreatment at 873 K slightly decreased the crystalline size of TiO_2 in the Ba/TiO_2 photocatalyst from 7.7 to 12 nm, although this value largely decreased for the TiO_2 photocatalyst. This result clearly indicates that the Ba modification suppressed the growth of TiO_2 particles. Similar effects were previously reported for metal doping into TiO_2 (e.g., Si, Zr,[35] La,[36] and Al[37]). The Ba loading enhanced the thermal stability of the catalyst, which should be one of the reasons for the higher NSC of the Ba/TiO_2 catalyst than that of the TiO_2 catalyst. The thermal stability is an advantage in the practical use of lean-burn engines.

The effect of the pretreatment temperature on the activity of the Ba/TiO_2 catalyst is summarized in Table 1. In the pretreatment temperature range of 298−573 K, the NSC of the Ba/TiO_2 catalyst (entries 4−6 in Table 1) was lower than that of the bare TiO_2 catalyst after the pretreatment at 773 K (entry 2) even though the crystalline size of TiO_2 in the Ba/TiO_2 catalyst was smaller than that in the TiO_2 catalyst. The generation of crystalline $Ba(NO_3)_2$ was observed in the as-prepared Ba/TiO_2 catalyst using XRD (Figure 3), which

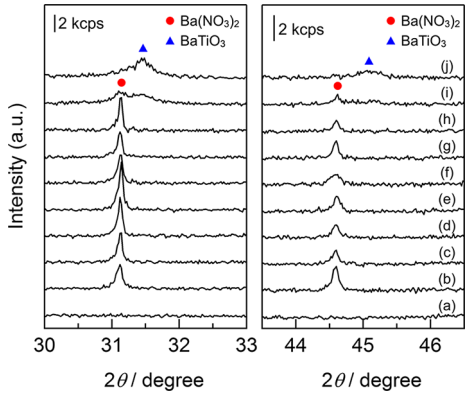

Figure 3. XRD patterns of the catalysts before and after the reaction at various pretreatment temperatures. (a) as-synthesized TiO_2, (b) as-synthesized Ba/TiO_2, and Ba/TiO_2 after the reaction at the pretreatment temperatures of (c) 298 K, (d) 473 K, (e) 573 K, (f) 623 K, (g) 673 K, (h) 723 K, (i) 773 K, and (j) 873 K. XRD patterns in the range of 2θ = 10−70 degree are shown in Figure S5 in SI.

suggests that the decrease in the NSC occurs because the TiO_2 surface is covered with the impregnated $Ba(NO_3)_2$ species. The NSC increased drastically upon increasing the pretreatment temperature from 573 to 673 K. The increase in the NSC was not due to the change in the SSA because the SSA decreased from 187 to 155 $m^2\ g^{-1}$. The crystalline size of TiO_2 did not change in the pretreatment temperature region of 573−673 K, which indicates that the growth of TiO_2 particles did not occur during the pretreatment in this temperature region. To investigate the effect of the pretreatment temperature, temperature programed desorption (TPD) experiments were

Table 1. Result of the NO_x Storage, the BET Specific Surface Area, and the Crystalline Size of the TiO_2 Particle

			SSA[b]/$m^2\ g^{-1}$		d[c]/nm		NSC[f]	dead time[g]
entry	catalyst	temp[a]/K	as-syn.[d]	AR[e]	as-syn.[d]	AR[e]	/ μmol g^{-1}	/ s
1	TiO_2	673	292	235	7.7	8.9	203	573
2	TiO_2	773	292	185	7.7	11	177	530
3	TiO_2	873	292	50.7	7.7	28	83.6	58
4	Ba/TiO_2[h]	298	180	188	7.7	7.9	156	97
5	Ba/TiO_2[h]	473	180	188	7.7	7.8	124	33
6	Ba/TiO_2[h]	573	180	187	7.7	8.0	108	100
7	Ba/TiO_2[h]	623	180	166	7.7	7.9	125	170
8	Ba/TiO_2[h]	673	180	155	7.7	8.3	230	727
9	Ba/TiO_2[h]	723	180	166	7.7	8.3	228	629
10	Ba/TiO_2[h]	773	180	154	7.7	8.8	225	650
11	Ba/TiO_2[h]	873	180	108	7.7	12	175	306

[a]Pretreatment temperature. [b]Specific surface area determined by the BET methods. [c]Crystalline size of the TiO_2 particles. [d]As-synthesized. [e]After the NO_x storage reaction. [f]NO_x storage capacity after 1 h of the reaction. [g]Reaction time after which the outlet concentration of NO_x was less than 2 ppm. [h]Ba loading: 1000 μmol g^{-1}.

DOI: 10.1021/acscatal.5b00151
ACS Catal. 2015, 5, 2939−2943

performed using the same experimental setup as the reaction in a 10% O_2/He gas mixture, and the result of the as-prepared Ba/TiO_2 catalysts is presented in Figure 4 (experimental details in the SI). By integrating the TPD profiles, the total desorption amount of NO_x (NO + NO_2) was calculated to be 242 μmol, which was consistent with the loading amount of NO_3^- ions in the Ba/TiO_2 catalyst (260 μmol). The TPD spectrum was reasonably fitted using three Gaussian functions with peaks at 694, 806, and 840 K (the fitting result is presented in Figure S4). The intensity of crystalline $Ba(NO_3)_2$ in Figure 3 decreased after the pretreatment at 773 K and completely disappeared at 873 K. The XRD results reveal that the TPD peaks at the higher temperatures of 806 and 840 K were due to the decomposition of crystalline $Ba(NO_3)_2$ observed in the XRD patterns. The peak at temperatures below 694 K can possibly be attributed to $Ba(NO_3)_2$ on the TiO_2 surface. The desorption of NO started at approximately 600 K, which corresponded to the uptake temperature of the NSC of 623 K. The generation of NO was observed in TPD experiments, as shown in Figure 4. In addition, the concentration of NO in thermal equilibrium was calculated using the concentration of NO_x and O_2 (3%) (TPD experimental condition) and thermodynamic parameters of the following equation from the NIST Chemistry WebBook:[38]

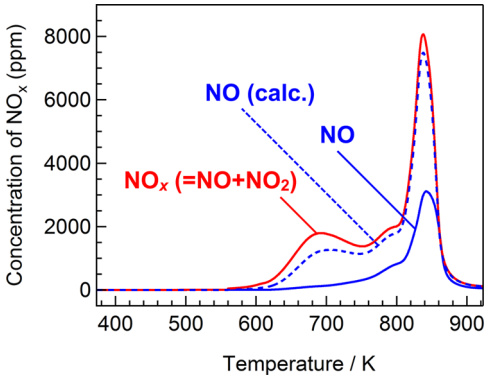

Figure 4. TPD profiles of 1000 μmol g^{-1} Ba/TiO_2 catalyst in a 10% O_2/He gas mixture. NO (calc.) was calculated using the equilibrium constants of eq 5 and the concentration of NO_x and O_2 (3%) in the TPD experiment.

$$NO + 1/2O_2 \rightleftarrows NO_2 \quad K = P_{NO2}/P_{NO}P_{O2}^{1/2} \tag{5}$$

where, P_x is the partial pressure of species x. The concentration of NO detected was much lower than that calculated especially at temperatures below 760 K, which indicates that NO_2 was first generated at temperatures below 850 K. Thus, the decomposition of $Ba(NO_3)_2$ proceeds as described in the following reaction.[39,40]

$$Ba(NO_3)_2 \rightarrow BaO + 2NO_2 + 1/2O_2 \tag{6}$$

Thus, we concluded that the increase of the NSC between 623 and 673 K was due to the generation of BaO, as observed in eq 6, and the generated BaO functions as a NO_x storage material in the photoassisted NO_x storage as well as the typical NSR catalyst. The NSC decreased at the pretreatment temperature of 873 K. At this temperature, the SSA decreased, and the crystalline size of TiO_2 increased. In addition, the diffraction peaks of the $BaTiO_3$ mixed oxide appeared (Figure 3). Thus, the decrease in the NSC at 873 K could be due to the decrease in the SSA of the catalyst and/or the generation of the $BaTiO_3$ mixed oxide.

In summary, we have developed an effective NO_x storage method at a low temperature using TiO_2-based photocatalysts under UV-light irradiation. We observed that the Ba modification on a TiO_2 surface drastically improved the performance of the catalyst. The Ba/TiO_2 photocatalyst exhibited 1020 s of dead time, which is sufficient for the desired value (800 s) reported by the ICCT. The effect of the pretreatment temperature was also studied, and two positive effects of Ba modification on the NSC were proposed: (i) the Ba modification inhibits the densification of TiO_2 particles, which helped to maintain the high SSA of TiO_2 and (ii) the BaO species, which was generated from the decomposition of $Ba(NO_3)_2$, works as a NO_x storage material over the photocatalysts at low temperatures. We concluded that TiO_2 and Ba/TiO_2 are promising for NO_x storage materials at low temperatures and have the potential to reduce NO_x emissions in the cold start condition.

■ ASSOCIATED CONTENT

Supporting Information

The following file is available free of charge on the ACS Publications website at DOI: 10.1021/acscatal.5b00151.

Experimental details and results of the long-time reaction, XRD patterns of TiO_2 samples, and peak deconvolution of the TPD profile (PDF)

■ AUTHOR INFORMATION

Corresponding Authors

*(K.T.) E-mail: teramura@moleng.kyoto-u.ac.jp.
*(T.T.) E-mail: tanakat@moleng.kyoto-u.ac.jp.

Notes

The authors declare no competing financial interest.

■ ACKNOWLEDGMENTS

This study was partially supported by the Program for Element Strategy Initiative for Catalysts and Batteries (ESICB), commissioned by the Ministry of Education, Culture, Sports, Science, and Technology (MEXT) of Japan, and the Precursory Research for Embryonic Science and Technology (PRESTO), supported by the Japan Science and Technology Agency (JST). A.Y. thanks the JSPS Research Fellowships for Young Scientists.

■ REFERENCES

(1) Takahashi, N.; Shinjoh, H.; Iijima, T.; Suzuki, T.; Yamazaki, K.; Yokota, K.; Suzuki, H.; Miyoshi, N.; Matsumoto, S.-i.; Tanizawa, T.; Tanaka, T.; Tateishi, S.-s.; Kasahara, K. *Catal. Today* **1996**, *27*, 63−69.
(2) Centi, G.; Arena, G. E.; Perathoner, S. *J. Catal.* **2003**, *216*, 443−454.
(3) Kašpar, J.; Fornasiero, P.; Hickey, N. *Catal. Today* **2003**, *77*, 419−449.
(4) Koebel, M.; Elsener, M.; Kleemann, M. *Catal. Today* **2000**, *59*, 335−345.
(5) Baik, J.; Yim, S.; Nam, I.-S.; Mok, Y.; Lee, J.-H.; Cho, B.; Oh, S. *Top. Catal.* **2004**, *30−31*, 37−41.
(6) Fridell, E.; Skoglundh, M.; Westerberg, B.; Johansson, S.; Smedler, G. *J. Catal.* **1999**, *183*, 196−209.
(7) Lietti, L.; Forzatti, P.; Nova, I.; Tronconi, E. *J. Catal.* **2001**, *204*, 175−191.
(8) Corbos, E. C.; Haneda, M.; Courtois, X.; Marecot, P.; Duprez, D.; Hamada, H. *Appl. Catal., A* **2009**, *365*, 187−193.

DOI: 10.1021/acscatal.5b00151
ACS Catal. 2015, 5, 2939−2943

(9) Sullivan, J. A.; Cunningham, J.; Morris, M. A.; Keneavey, K. *Appl. Catal., B* **1995**, *7*, 137−151.
(10) Busca, G.; Lietti, L.; Ramis, G.; Berti, F. *Appl. Catal., B* **1998**, *18*, 1−36.
(11) Long, R. Q.; Yang, R. T. *J. Am. Chem. Soc.* **1999**, *121*, 5595−5596.
(12) Ma, A.-Z.; Grunert, W. *Chem. Commun.* **1999**, 71−72.
(13) Long, R. Q.; Yang, R. T. *J. Catal.* **2002**, *207*, 274−285.
(14) Liu, G.; Gao, P.-X. *Catal. Sci. Technol.* **2011**, *1*, 552−568.
(15) Epling, W. S.; Campbell, L. E.; Yezerets, A.; Currier, N. W.; Parks, J. E. *Catal. Rev.: Sci. Eng.* **2004**, *46*, 163−245.
(16) Dana, L.; Fanta, K. *Urban off-cycle NOx emissions from Euro IV/V trucks and buses*; International Council on Clean Transportation: San Fransisco, 2012; http://www.theicct.org/urban-cycle-nox-emissions-euro-ivv-trucks-and-buses.
(17) Takahashi, N.; Yamazaki, K.; Sobukawa, H.; Shinjoh, H. *Appl. Catal., B* **2007**, *70*, 198−204.
(18) Li, J.; Chang, H.; Ma, L.; Hao, J.; Yang, R. T. *Catal. Today* **2011**, *175*, 147−156.
(19) Dalton, J. S.; Janes, P. A.; Jones, N. G.; Nicholson, J. A.; Hallam, K. R.; Allen, G. C. *Environ. Pollut.* **2002**, *120*, 415−422.
(20) Yin, S.; Yamaki, H.; Komatsu, M.; Zhang, Q.; Wang, J.; Tang, Q.; Saito, F.; Sato, T. *Solid State Sci.* **2005**, *7*, 1479−1485.
(21) Ohko, Y.; Nakamura, Y.; Negishi, N.; Matsuzawa, S.; Takeuchi, K. *J. Photochem. Photobiol., A* **2009**, *205*, 28−33.
(22) Hashimoto, K.; Sumida, K.; Kitano, S.; Yamamoto, K.; Kondo, N.; Kera, Y.; Kominami, H. *Catal. Today* **2009**, *144*, 37−41.
(23) Hashimoto, K.; Wasada, K.; Osaki, M.; Shono, E.; Adachi, K.; Toukai, N.; Kominami, H.; Kera, Y. *Appl. Catal., B* **2001**, *30*, 429−436.
(24) Hashimoto, K.; Wasada, K.; Toukai, N.; Kominami, H.; Kera, Y. *J. Photochem. Photobiol., A* **2000**, *136*, 103−109.
(25) Lasek, J.; Yu, Y.-H.; Wu, J. C. S. *J. Photochem. Photobiol., C* **2013**, *14*, 29−52.
(26) Ishibai, Y.; Sato, J.; Akita, S.; Nishikawa, T.; Miyagishi, S. *J. Photochem. Photobiol., A* **2007**, *188*, 106−111.
(27) Ballari, M. M.; Hunger, M.; Hüsken, G.; Brouwers, H. J. H. *Appl. Catal., B* **2010**, *95*, 245−254.
(28) Shelimov, B. N.; Tolkachev, N. N.; Tkachenko, O. P.; Baeva, G. N.; Klementiev, K. V.; Stakheev, A. Y.; Kazansky, V. B. *J. Photochem. Photobiol., A* **2008**, *195*, 81−88.
(29) Ibusuki, T.; Takeuchi, K. *J. Mol. Catal.* **1994**, *88*, 93−102.
(30) Dillert, R.; Engel, A.; Gro; Lindner, P.; Bahnemann, D. W. *Phys. Chem. Chem. Phys.* **2013**, *15*, 20876−20886.
(31) Folli, A.; Campbell, S. B.; Anderson, J. A.; Macphee, D. E. *J. Photochem. Photobiol., A* **2011**, *220*, 85−93.
(32) Wu, Q.; van de Krol, R. *J. Am. Chem. Soc.* **2012**, *134*, 9369−9375.
(33) Hadjiivanov, K.; Knozinger, H. *Phys. Chem. Chem. Phys.* **2000**, *2*, 2803−2806.
(34) Hadjiivanov, K. I. *Catal. Rev.: Sci. Eng.* **2000**, *42*, 71−144.
(35) Fu, X.; Clark, L. A.; Yang, Q.; Anderson, M. A. *Environ. Sci. Technol.* **1996**, *30*, 647−653.
(36) Liqiang, J.; Xiaojun, S.; Baifu, X.; Baiqi, W.; Weimin, C.; Honggang, F. *J. Solid State Chem.* **2004**, *177*, 3375−3382.
(37) Soylu, A. M.; Polat, M.; Erdogan, D. A.; Say, Z.; Yıldırım, C.; Birer, Ö.; Ozensoy, E. *Appl. Surf. Sci.* **2014**, *318*, 142−149.
(38) *The NIST Chemistry WebBook*; Linstrom, P., Mallard, W., Eds.; National Institute of Standards and Technology: Gaithersburg, MD, 2011; http://webbook.nist.gov (accessed November 2, 2014).
(39) Zhou, G.; Luo, T.; Gorte, R. J. *Appl. Catal., B* **2006**, *64*, 88−95.
(40) Wang, X.; Yu, Y.; He, H. *Appl. Catal., B* **2010**, *100*, 19−30.

DOI: 10.1021/acscatal.5b00151
ACS Catal. 2015, 5, 2939−2943